Article

Exciton Energy Transfer-Assisted Photoluminescence Brightening from Freestanding Single-Walled Carbon Nanotube Bundles

Toshiaki Kato, and Rikizo Hatakeyama

J. Am. Chem. Soc., **2008**, 130 (25), 8101-8107 • DOI: 10.1021/ja802427v • Publication Date (Web): 31 May 2008

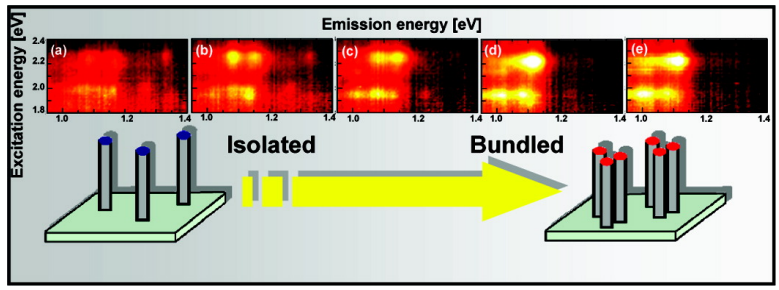

More About This Article

Additional resources and features associated with this article are available within the HTML version:

- Supporting Information
- Links to the 2 articles that cite this article, as of the time of this article download
- Access to high resolution figures
- Links to articles and content related to this article
- Copyright permission to reproduce figures and/or text from this article

View the Full Text HTML

J|A|C|S
ARTICLES

Published on Web 05/31/2008

Exciton Energy Transfer-Assisted Photoluminescence Brightening from Freestanding Single-Walled Carbon Nanotube Bundles

Toshiaki Kato* and Rikizo Hatakeyama

Department of Electronic Engineering, Tohoku University, Aoba 6-6-05, Aramaki-Aza, Aoba-Ku, Sendai, Japan

Received April 3, 2008; E-mail: kato12@ecei.tohoku.ac.jp

Abstract: Photoluminescence (PL) brightening is clearly observed through the direct morphology transition from isolated to thin bundled vertically- and individually freestanding single-walled carbon nanotubes (SWNTs). On the basis of the precise spectra analysis and equation-based estimation of the PL time trace, the origin of the PL brightening is consistently explained in terms of the exciton energy transfer through the tube bundles. The PL brightening is also revealed to obviously depend on SWNT diameters. Only the small-diameter rich sample can realize the PL brightening, which can be explained by the different concentrations of metallic SWNTs causing a PL quenching. Since it can be possible to fabricate brightly illuminating nanotubes on various kinds of substrates, the bundle engineering with freestanding nanotubes is expected to be a potential candidate for realizing the nanotube-based PL device fabrication.

Introduction

The optical property of single-walled carbon nanotubes (SWNTs)[1] has been the subject of intense interest in recent years, since the discovery of efficient photoluminescence (PL) from isolated semiconducting SWNTs.[2] Because it was believed that the debundle of SWNTs was the inevitable process to capture the PL signal from SWNTs, the bundle forming SWNTs was, in most cases, treated as byproduct or impurities causing a spectra broadening and shifting, and hence their optical features, especially the PL, have not attracted a great deal of attention thus far. Very recently, the PL from bundled SWNTs in an aqueous solution has been reported.[3,4] Since the PL from bundled SWNTs includes outstanding advantages such as an exemption of a complicated debundle process and easy manipulation, it can be expected that the SWNT bundle engineering has a great potential aiming for the nanotube-based PL device fabrication. From an industrial point of view, the application of nanotube PL to the well-organized present semiconductor technology is an inevitable factor (i.e., the establishment of bright PL emission from a solid-state material is regarded to be a still remaining fundamental problem). Up to now, promising PL features from the solid-state sample were reported using individual SWNTs such as SWNTs suspending between pillars,[5] high quality SWNTs,[6] and SWNT composite.[7] Although several measurements on the PL with a vertically aligned SWNT film were reported, any concrete implications of the bundle formation for the PL have not been discussed thus far.[8] Herein, we report unique PL features from as-grown freestanding SWNT bundles produced by diffusion plasma chemical vapor deposition (DPCVD).[9] The outstanding increment of the PL intensity is observed through the direct morphology transition from isolated to bundled SWNTs, and such PL peak changes can well be explained in terms of the exciton energy transfer (EET) model.[3] The continuous equation for the time evolution of integrated PL intensity between isolated and bundled SWNTs also provides efficient evidence for the PL brightening through the EET in bundle. The dependence of macroscopic EET efficiency ($\varepsilon_{m\text{-}EET}$) on the tube diameter distribution is also discussed, and several important factors realizing the PL brightening are argued. Since the brightly illuminating freestanding SWNT bundles can directly be grown on various kinds of substrates, they are expected to greatly contribute to realizing nanotube-base PL device applications.

Sample Preparation and Experimental Methods

A homemade DPCVD system was utilized for the growth of freestanding SWNTs.[9] The iron (thickness (t) = 0.5−1 nm)/Al_2O_3 (t = 20 nm) multilayer catalyst was formed on a silver substrate (t = 0.2 mm) by a vacuum evaporation and a sputtering method, respectively. For the direct observation of the as-grown state of SWNTs with transmission electron microscopy (TEM, Hitachi HF-

(1) Iijima, S.; Ichihashi, T. *Nature* **1993**, *363*, 603.
(2) (a) O'Connell, M. J.; Bachilo, S. M.; Huffman, C. B.; Moore, V. C.; Strano, M. S.; Haroz, E. H.; Rialon, K. L.; Boul, P. J.; Noon, W. H.; Kittrell, C.; Ma, J.; Hauge, R. H.; Weisman, R. B.; Smalley, R. E. *Science* **2002**, *297*, 593. (b) Bachilo, S. M.; Strano, M. S.; Kittrell, C.; Hauge, R. H.; Smalley, R. E.; Weisman, R. B. *Science* **2002**, *298*, 2361.
(3) Torrens, O. N.; Milkie, D. E.; Zheng, M.; Kikkawa, J. M. *Nano Lett.* **2006**, *6*, 2864.
(4) Tan, P. H.; Rozhin, A. G.; Hasan, T.; Hu, P.; Scardaci, V.; Milne, W. I.; Ferrari, A. C. *Phys. Rev. Lett.* **2007**, *99*, 137402.
(5) Lefebvre, J.; Homma, Y.; Finnie, P. *Phys. Rev. Lett.* **2003**, *90*, 217401.
(6) Okazaki, T.; Saito, T.; Matsuura, K.; Ohshima, S.; Yumura, M.; Iijima, S. *Nano Lett.* **2005**, *5*, 2618.
(7) Kim, Y.; Minami, S.; Kazaoui, S. *Appl. Phys. Lett.* **2005**, *86*, 073103.
(8) (a) Hata, K.; Futaba, D. N.; Mizuno, K.; Namai, T.; Yumura, M.; Iijima, S. *Science* **2004**, *306*, 1362. (b) Kiowski, O.; Lebedkin, S.; Hennrich, F.; Malik, S.; Rösner, H.; Arnold, K.; Sürgers, C.; Kappes, M. M. *Phys. Rev. B* **2007**, *75*, 075421.
(9) Kato, T.; Hatakeyama, R.; Tohji, K. *Nanotechnology* **2006**, *17*, 2223.

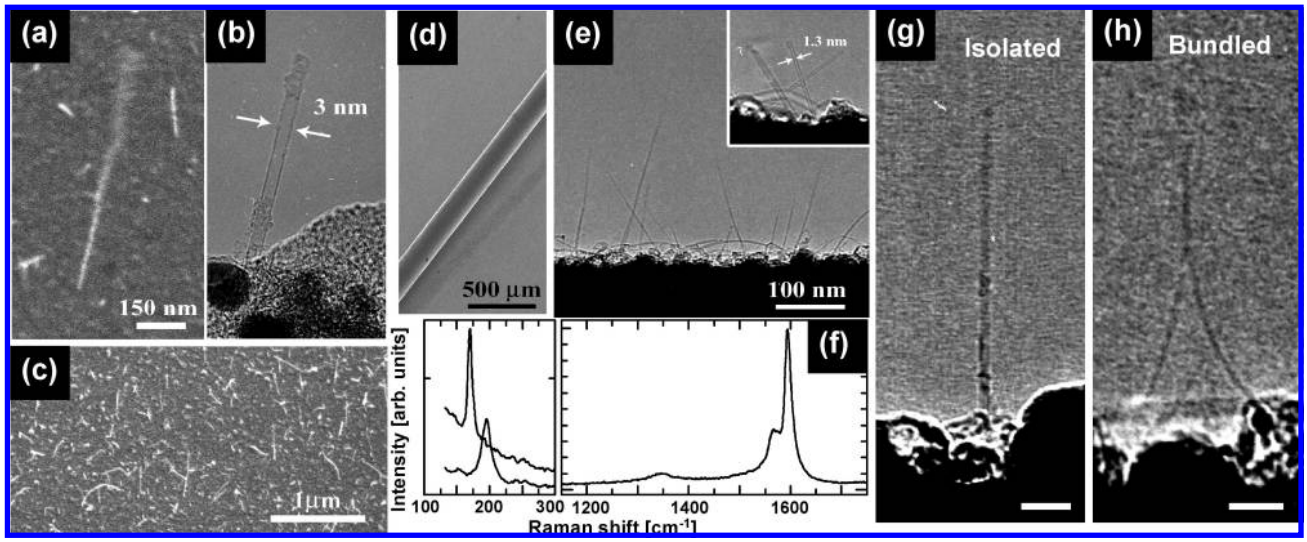

Figure 1. Typical high-magnification SEM (a), TEM image (b), and low-magnification SEM image of freestanding SWNTs grown on a flat substrate. (d) Low-magnification SEM image of thin Cu wire utilized for direct TEM observation. (e) Direct TEM observation of freestanding individual SWNTs grown on thin Cu wire. Inset shows high magnification TEM image. (f) Raman scattering spectrum of freestanding SWNTs. Lower Raman shift area indicates typical sharp RBM from two different samples. Typical TEM images of isolated (g) and thin bundled (f) freestanding SWNTs, respectively. (f, g) Scale bar shows 20 nm.

2000) operated at 200 keV, a copper thin wire (diameter = 100 μm) covered by the multilayer catalyst was utilized. The Raman scattering spectroscopy, excitation wavelength was fixed at 488 nm, was used for the quality and diameter analysis. PL measurements were performed with a JY (Horiba) Fluorolog-3 system. The excitation wavelength was varied from 500 to 850 nm in 4-nm steps, and emission signals were accumulated for 20 s in each excitation step. Excitation and emission slit widths were fixed at 10 nm. To cut the Rayleigh scattering, optical filters (Sigmakoki, ITF-50S-83IR, ITF-50S-85IR) were set in front of a liquid nitrogen-cooled InGaAs array detector. For the polarized PL measurement, a UV−vis−NIR polarizer (Sigmakoki, SPF-30C-32) and a NIR polarizer (Sigmakoki, SPFN-30C-26) were set behind the excitation and in front of the emission monochromator, respectively (see Supporting Information for details).

Results and Discussion

Figure 1 shows typical scanning electron microscope (SEM, Hitachi S-4100), TEM images, and Raman scattering spectra of freestanding SWNTs fabricated with a DPCVD method. SWNTs are found to be grown on a whole range of flat substrate surfaces (Figure 1a−c). To directly observe the as-grown state of SWNTs with TEM, the thin Cu wire (100 μm) covered by the above-mentioned catalyst layer (Fe/Al_2O_3) was utilized as a substrate (Figure 1d). Plenty of SWNTs with a few hundred nanometers in length are found to vertically stand on a substrate surface owing to a strong plasma sheath electric field during their growth (Figure 1e).[9] The large dipole moment in SWNTs caused by the plasma sheath electric field is accompanied by a high rotation energy, making each nanotube vertically stand without being supported by neighboring SWNTs like in SWNT films. Since an ion energy coming into a substrate can be strongly decreased in a diffusion area of plasmas, strong ion-bombardment effects resulting in significant damages on a tube structure can be restricted. Thus, damage-free high-quality SWNT growth can be realized as recognized from the low D-band (1250−1400 cm^{-1}) intensity of Raman scattering spectra in Figure 1f.[10] The sharp radial breathing mode (RBM) in a lower Raman shift area (100−300 cm^{-1}) also indicates the growth of individual SWNTs (Figure 1f).[11] It is worthwhile to mention that, in addition to the completely freestanding individual SWNTs (Figure 1g), a few SWNTs forming a thin bundlelike structure were also often observed during the direct TEM observation (Figure 1h). These unique morphology differences, completely isolated or thin bundled freestanding SWNTs, are found to obviously affect their optical features (see below for details).

A photoluminescence excitation (PLE) map derived from as-grown freestanding SWNTs and typical emission spectra at primal bright spots in the PLE map are plotted in Figure 2a,b, respectively. On the basis of each precisely analyzed spectrum, it is found that those spectra consist of two different sharp and broad peaks. Circles in Figure 2b mark the Lorentzian peaks with a relatively sharp average width (26.8 meV). Almost every sharp peak is clearly blue-shifted by about 60 meV in both the excitation and emission energies compared with the result of sodium dodecyl sulfate (SDS) wrapped SWNTs (the detailed values for each chirality are listed in Table 1).[12] These PL features such as a sharp Lorentzian shape and clear blue-shifting of excitation and emission energies are well matched with the previously reported PL spectra from air-suspended individual SWNTs between pirals.[5] Furthermore, only the polarized excitation parallel to the tube axis induces a bright PL emission as described in Figure 2c,d (see the Supporting Information for details). On the basis of the PL behaviors demonstrated, it can be deduced that the PL captured comes from the freestanding individual SWNTs. Noticeably, by contrast, it is also found that there are several broad peaks marked as triangles in Figure 2b, and their origin cannot be identified with the simple blue-shifting estimation as mentioned above.

(10) Kato, T.; Hatakeyama, R. *Appl. Phys. Lett.* **2008**, *92*, 031502.

(11) (a) Jorio, A.; Saito, R.; Hafner, J. H.; Lieber, C. M.; Hunter, M.; McClure, T.; Dresselhaus, G.; Dresselhaus, M. S. *Phys. Rev. Lett.* **2001**, *86*, 1118. (b) Jorio, A.; Filho, A. G. S.; Dresselhaus, G.; Dresselhaus, M. S.; Saito, R.; Hafner, J. H.; Lieber, C. M.; Matinaga, F. M.; Dantas, M. S. S.; Pimenta, M. A. *Phys. Rev. B* **2001**, *63*, 245416.

(12) Weisman, R. B.; Bachilo, S. M. *Nano Lett.* **2003**, *3*, 1235.

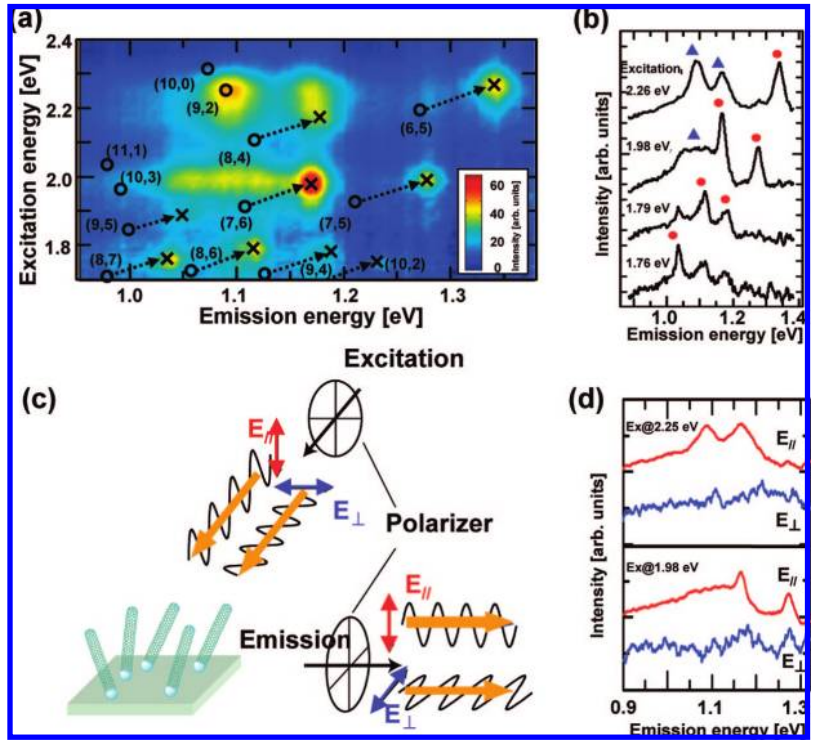

Figure 2. PLE map (a) and typical emission spectra (b) measured from as-grown freestanding individual SWNTs. ○ and × in (a) show the positions of SDS-wrapped SWNTs (data from ref 12) and our chirality-assigned peaks, respectively. ● and ▲ in (b) mark sharp (chirality-assigned) and broad (unknown) peaks, respectively. Schematic illustration of polarized PL measurement (c) and typical emission spectra (d) measured by parallel ($E_{//}$) and perpendicular ($E_{\perp}$) polarized light source against the tube axis (see Supporting Information for experimental details).

Table 1. ΔE_{11}, ΔE_{22}, and E_{11}/E_{22} for Each Chirality Nanotube and Averaged Data[a]

	$\Delta E_{ii} = E_{ii}$(freestanding) − E_{ii}(SDS)		
(*n*,*m*)	ΔE_{11} (meV)	ΔE_{22} (meV)	E_{22}/E_{11}
(6,5)	69.0	72.0	1.69
(7,5)	65.8	64.7	1.56
(7,6)	62.5	60.9	1.69
(8,6)	57.5	64.9	1.61
(8,7)	54.5	58.1	1.70
(9,4)	61.1	64.2	1.50
(9,5)	48.5	45.0	1.80
average	59.9	61.4	1.65

[a] ΔE_{ii} is denoted by the following correlation: $\Delta E_{ii} = E_{ii}$(freestanding) − E_{ii}(SDS), where E_{ii}(freestanding) and E_{ii}(SDS) are PL peak positions of our experimental data and SDS wrapped SWNTs (data from ref [12]), respectively.

To uncover the origin of such unknown peaks, we considered the availability of the EET model.[3] Figure 3 exhibits the PLE map, contour plot, and several excitation and emission spectra relating to the unknown broad peaks, respectively. The excitation energies of broad peaks A (= B) and C in the PLE map of Figure 3 are about 2.25 and 1.99 eV, which match fairly well with those of (6,5) and (7,6), respectively. Additionally, the emission energy of A corresponds to that of (7,6) or (8,4). Such correlation between the excitation and emission energies indicates that the resonant exciton of large gap (6,5) induces emission from smaller gap tubes such as (7,6) and (8,4) as a result of the bundle formation. This can be considered as the origin of broad peak A based on the EET model. Although it is difficult to completely identify the acceptor tube for the other two peaks B and C because of the existence of several peaks having emission energies similar to those of B and C, the clear correspondence of the excitation energy between B (C) and (6,5) ((7,5) or (7,6)) claims that the origin of those broad peaks might also be the EET. The EET model explained above seems to correspond well with our experimental results. However, it should be mentioned that the low energy level caused by intertube contact and interaction[13] can also be the candidate to explain the origin of the above-mentioned unknown broad peaks. To obtain more detailed evidence for the EET through the tube bundle in our results, therefore, the time evolution PLE measurement and its quantitative analysis based on simple equations are carried out.

Figure 4a shows the PLE map of as-grown freestanding SWNTs as a function of time passage after their growth (the PL measurement was immediately performed just after the time when samples were taken out from the vacuum chamber, which is denoted by 0 h). The excitation energy was set in the resonant range for the (6,5) tube (2.1−2.4 eV), where two clear PL peaks were observed at different emission energy areas. The sharp one is from the (6,5) tube, and the other broad one is the unknown origination as mentioned in Figures 2 and 3. Surprisingly, those two-peak intensities are changed linking with each other and seem to follow some hidden special rules. With an increase in the passage of time, the intensity of the (6,5) peak drastically decreases and downshifts about 50 meV. In contrast, the original broad peak intensities become obviously strong with passing time (Figure 4a). To reveal more concrete correlations between those two peaks, we carried out the detailed spectra analysis for each peak. Figures 4b gives the typical raw emission spectra and their Lorentzian fitting curves. The excitation energy was set at the highest PL intensity of the (6,5) tube, and the emission spectra were resolved into several Lorentzian com-

(13) Scholes, G. D.; Tretiak, S.; McDonald, T. J.; Metzger, W. K.; Engtrakul, C.; Rumbles, G.; Heben, M. J. *J. Phys. Chem. C* **2007**, *111*, 11139.

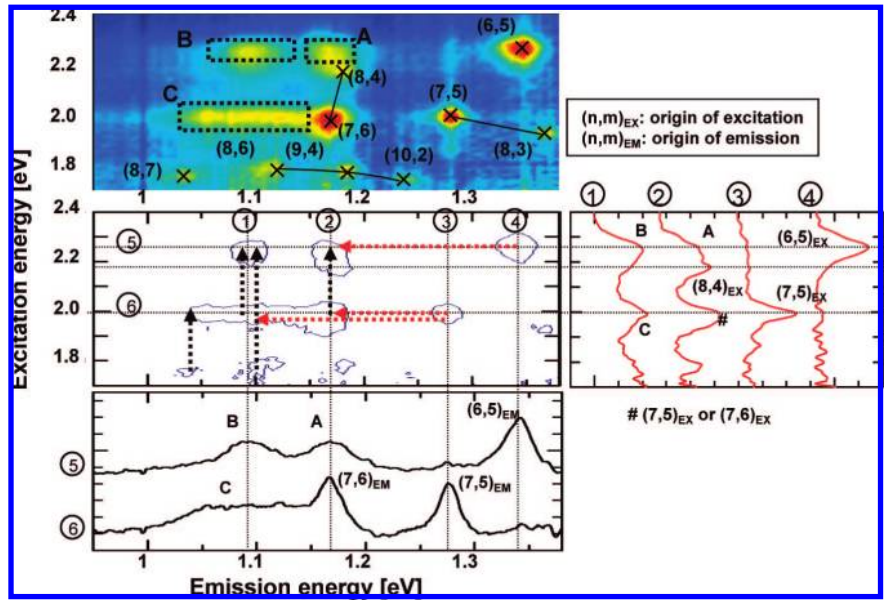

Figure 3. PLE map, counter plot, and several excitation and emission spectra relating to the broad peaks described as A, B, and C in the PLE map measured immediately after the growth. Solid lines in the PLE map show family patterns of chirality-assigned SWNTs.

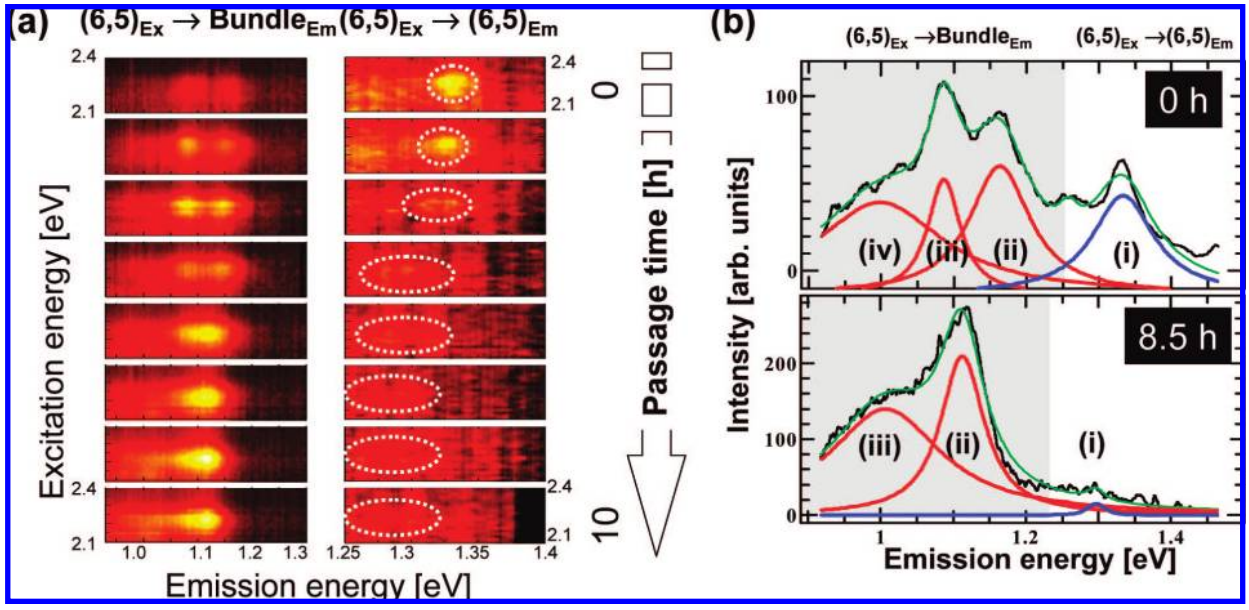

Figure 4. (a) Time evolution of the PLE map from as-grown freestanding SWNTs. Left and right parts are emissions from bundled SWNTs and isolated (6,5) nanotubes, respectively. The time traces of PLE map for each bundled (left) and isolated (right) SWNTs are shown with the same color scale. (b) Time evolution of raw emission spectra (black), multipeak fitting curve (green), and each Lorentzian component (blue and red) measured from freestanding SWNTs (upper and lower ones are 0 and 8.5 h after the growth). (i) and (ii−iv) are emissions from (6,5) tubes and bundled SWNTs, respectively.

ponents with a multipeak fitting function as described in Figure 4b. Peaks (i) and (ii−iv) were assigned as PL from the isolated (6,5) tubes and unknown broad peaks. An integral peak intensity (i) and summation of integral peak intensities (ii−iv) in the emission energy range are denoted as $I_{\mathrm{int}(6,5)\rightarrow(6,5)}$ and $I_{\mathrm{int}(6,5)\rightarrow\mathrm{bundle}}$, respectively. When we compared the two time traces of those spectra from 0 to 8.5 h, we found that the (i) and (ii−iv) peaks seem to have an inverse correlation, which can be well explained by the following equation-based estimation.

The PL intensity from SWNT per unit length ($I_\varepsilon(\varepsilon)$) can be described with the following equation:[14]

$$I_\varepsilon(\varepsilon) \propto W_{\mathrm{ab}} W_{\mathrm{rel}}(\varepsilon) W_{\mathrm{em}}(\varepsilon) \qquad (1)$$

where ε, W_{ab}, $W_{\mathrm{rel}}(\varepsilon)$, and $W_{\mathrm{em}}(\varepsilon)$ are emission energy, absorption efficiency, transition probability from E_{22} to E_{11}, and recombination rate, respectively. The total intensity from "A" chirality nanotubes in a sample can be denoted by the integration of $I_\varepsilon(\varepsilon)$ in the emission energy range, which has the following form:

$$I_{\mathrm{int}}(t)_{\mathrm{A}} \propto S(t)_{\mathrm{A}} \int_{\varepsilon_{\mathrm{l}}}^{\varepsilon_{\mathrm{h}}} I_\varepsilon(\varepsilon)_{\mathrm{A}}\, \mathrm{d}\varepsilon \qquad (2)$$

where $S(t)_{\mathrm{A}}$, ε_{l}, and ε_{h} are the effective surface area of SWNTs acting for PL emission in the tube "A", and lowest and highest

(14) Miyauchi, Y. Ph.D. Thesis, University of Tokyo, Japan, 2006.

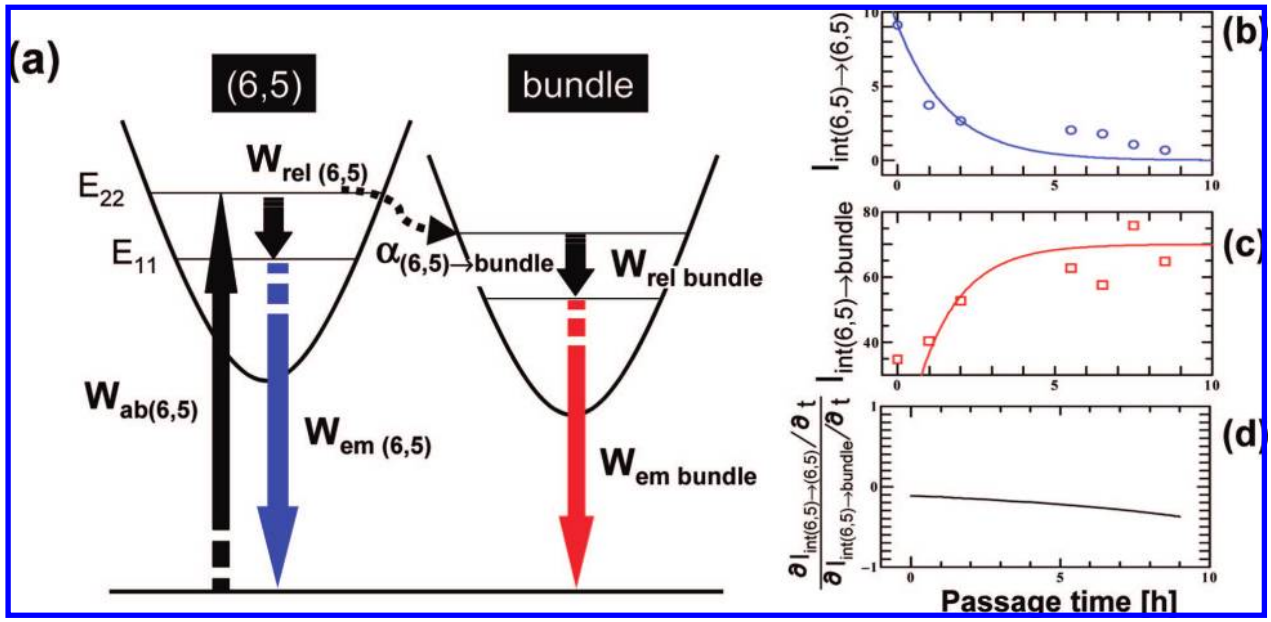

Figure 5. (a) Schematic model of the EET between (6,5) and bundled SWNTs. The time dependence of total intensity of (6,5) (b) and bundled (c) SWNTs excited at (6,5) tubes (○ and □ mark experimental data, and solid lines are fitting curves), and their time differential ratio (d).

emission energies, respectively. The total intensity from individual (6,5) tubes and bundled nanotubes including (6,5) tubes excited at the E_{22} resonance energy of (6,5) can be written as follows:

$$I_{\mathrm{int}}(t)_{(6,5)\rightarrow(6,5)} \propto S(t)_{(6,5)} W_{\mathrm{ab}(6,5)} \int_{\varepsilon_1}^{\varepsilon_h} W_{\mathrm{rel}(6,5)}(\varepsilon) W_{\mathrm{em}(6,5)}(\varepsilon)\, \mathrm{d}\varepsilon \tag{3}$$

$$I_{\mathrm{int}}(t)_{(6,5)\rightarrow\mathrm{bundle}} \propto S(t)_{\mathrm{bundle}} W_{\mathrm{ab}(6,5)} \alpha_{(6,5)\rightarrow\mathrm{bundle}} \times \int_{\varepsilon_1}^{\varepsilon_h} W_{\mathrm{relbundle}}(\varepsilon) W_{\mathrm{embundle}}(\varepsilon)\, \mathrm{d}\varepsilon \tag{4}$$

where $\alpha_{(6,5)\rightarrow\mathrm{bundle}}$ is the EET efficiency from (6,5) to bundled nanotubes. In case of bundled SWNTs, the resonant exciton at (6,5) tube transfers to the lowest E_{11} nanotube, resulting in the PL emission (Figure 5a).

If the origin of broad peak is the intertube interaction and contact, there must be no clear correlations between the time evolution of $I_{\mathrm{int}(6,5)\rightarrow(6,5)}$ and $I_{\mathrm{int}(6,5)\rightarrow\mathrm{bundle}}$. On the other hand, if the resonant exciton at (6,5) tubes directly relates to the brightening of the broad peaks, the continuous correlation between $I_{\mathrm{int}(6,5)\rightarrow(6,5)}$ and $I_{\mathrm{int}(6,5)\rightarrow\mathrm{bundle}}$ must be satisfied, which is described in eq 5 (note that we assume that the time-dependent factor in eqs 3 and 4 is only $S(t)$):

$$\frac{\partial S(t)_{(6,5)}}{\partial t} + \frac{\partial S(t)_{\mathrm{bundle}}}{\partial t} = 0 \tag{5}$$

On the basis of the experimental results described in Figure 4a, the time evolution of total intensity was carefully analyzed and plotted in Figure 5b,c. In the case of $I_{\mathrm{int}(6,5)\rightarrow(6,5)}$, the total intensity is found to exponentially decay (Figure 5b). $I_{\mathrm{int}(6,5)\rightarrow\mathrm{bundle}}$ gradually increases as time passes, which can be described with the following equation (Figure 5c):

$$I_{\mathrm{int}(6,5)\rightarrow\mathrm{bundle}} = A\{1 - \exp[-(t - B)]\} \tag{6}$$

where A and B are fitting parameters.

From eqs 3 and 4, eq 5 can be converted into the following equation:

$$\frac{\partial I_{\mathrm{int}}(t)_{(6,5)\rightarrow(6,5)}}{\partial t} \Big/ \frac{\partial I_{\mathrm{int}}(t)_{(6,5)\rightarrow\mathrm{bundle}}}{\partial t} = \mathrm{const.} \tag{7}$$

Noticeably, when we plot the time-differential ratio between $I_{\mathrm{int}}(t)_{(6,5)\rightarrow(6,5)}$ and $I_{\mathrm{int}}(t)_{(6,5)\rightarrow\mathrm{bundle}}$, we found that the ratio is almost constant independently of the time passage (Figure 5d). This indicates that the continuous eq 5 is satisfied in our experimental result, and we can conclude that the resonant exciton (6,5) is directly transferred to the bundled nanotubes, resulting in the PL brightening. If the lower energy level made by the intertube interaction/contact is the critical answer for the broad spectra in the PLE map, it is impossible to explain the above-mentioned direct correlation between the depletion of the (6,5) peak and increment of broad peak as time passes.

Furthermore, the peak shift of the (6,5) tube described in Figure 4a is also consistent with the previous report that E_{11} and E_{22} become downshifting when a bundle structure is formed.[15] Interestingly, eq 6 is known as a Langmuir-type adsorption formula.[16] Since the time evolution of $I_{\mathrm{int}\ (6,5)\rightarrow\mathrm{bundle}}$ depends on $S(t)_{\mathrm{bundle}}$ (eq 4), the $S(t)_{\mathrm{bundle}}$ follows the Langmuir-type reaction in our result. This can also be explained by the consequence of the bundle formation because a bundling reaction can be assumed as a kind of adsorption reaction (i.e., carbon atoms on the surface of SWNTs adsorb the carbons in the other SWNTs through the bundle formation). On the basis of the above-mentioned discussion, it is believed that the origin of the broad peak in the PLE map is the EET through the tube bundles. It should be mentioned that the value of time differential of $I_{\mathrm{int}\ (6,5)\rightarrow(6,5)}$ compared to that of $I_{\mathrm{int}\ (6,5)\rightarrow\mathrm{bundle}}$ is the crucial factor directly related to the PL brightening. In our

(15) (a) Rao, A. M.; Chen, J.; Richter, E.; Schlecht, U.; Eklund, P. C.; Haddon, R. C.; Venkateswaran, U. D.; Kwon, Y.-K.; Tománek, D. *Phys. Rev. Lett.* **2001**, *86*, 3895. (b) Park, J. S.; Oyama, Y.; Saito, R.; Izumida, W.; Jiang, J.; Sato, K.; Fantini, C.; Jorio, A.; Dresselhaus, G.; Dresselhaus, M. S. *Phys. Rev. B* **2006**, *74*, 165414.
(16) Langmuir, I. *J. Am. Chem. Soc.* **1918**, *40*, 1361.

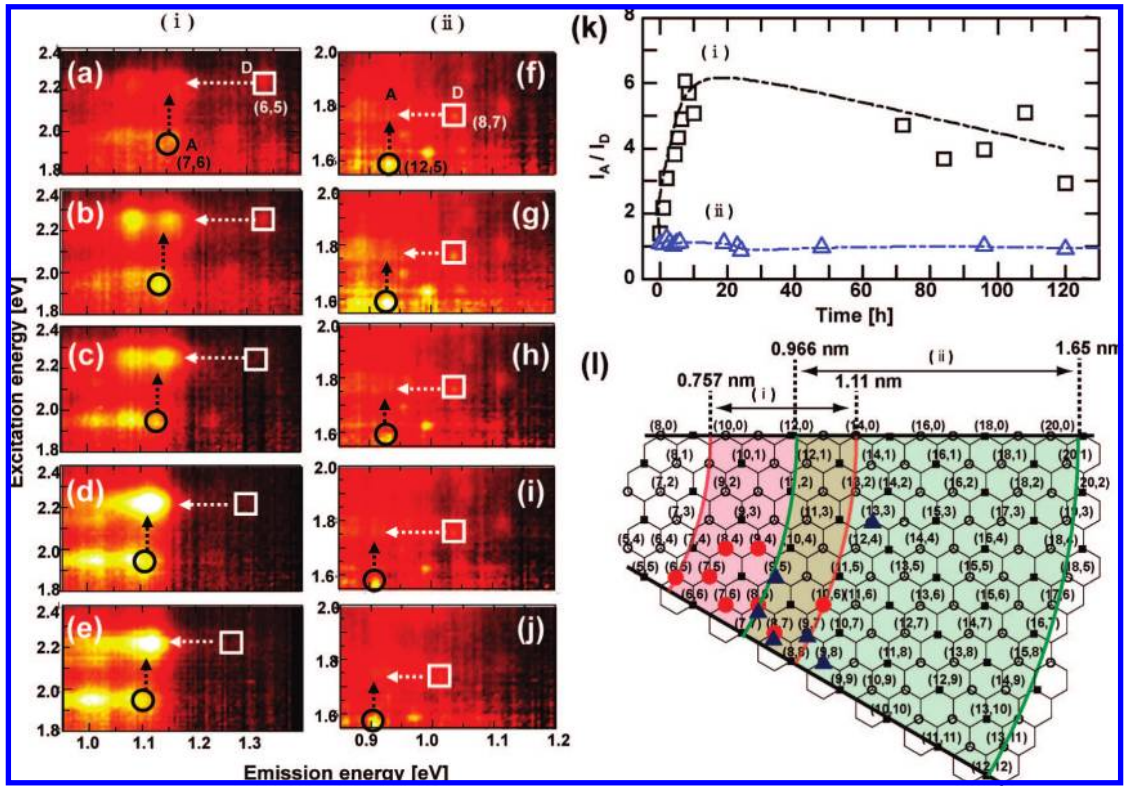

Figure 6. Time trace of the PLE map. (a−e) (f−j) PLE map of sample (i) (sample (ii)) measured at 0 h (0 h), 1 h (1 h), 3.5 h (4 h), 7.5 h (6 h), and 10 h (24 h) after the growth, respectively. □ and ○ mark the PL points of donor and acceptor tubes, respectively. Each PLE map (i) and (ii) is plotted with a same color scale. (k) I_A/I_D as a function of time passage. (l) Chirality distribution map of samples (i) and (ii). ○ and ■ describe semiconductor and metallic tubes, respectively. Detected chirality points in the PL measurement are described as ● (i) and ▲ (ii), respectively. The upper limit of diameter (ii) is calculated with RBM in Raman scattering spectra (Supporting Information).

measurement, the ratio is about 0.1−0.2 (Figure 5d), and it can be decided by the difference of integration parts in eqs 3 and 4 (maximum of $\alpha_{(6,5)\rightarrow bundle} \approx 1$). To address the perfect understanding of this point, further detailed theoretical and experimental work is required.

The most important question is why the PL was observed even forming bundle structures. To answer this question, the time trace of PLE as a function of SWNT diameter was investigated. As already discussed above, in the case of the small diameter sample, the PL brightening is definitely found as time passes (Figure 6a−e). Noticeably, however, no peak intensity change can be observed when the main diameter is large (Figure 6f−j). To quantitatively analyze these differences, we utilized the value of macroscopic EET efficiency $\varepsilon_{m\text{-}EET}$ denoted by the intensity ratio of acceptor (I_A) to donor (I_D) tubes[3] (note that the increment of $\varepsilon_{m\text{-}EET}$ does not indicate the improvement of SWNT quantum yield because the quantum yield of individual SWNT is directly decided only by their structure). Figure 6k shows the time evolution of I_A/I_D for samples with different diameter distributions. When the main diameter is relatively small ((i) 0.75−1.1 nm, calculated on the basis of the PL data), $\varepsilon_{m\text{-}EET}$ drastically increases to 6. Interestingly, in the case of large diameter nanotubes ((ii) 0.96−1.65),[17] I_A/I_D constantly kept the low value (∼1). This can be explained by the concentration difference of metallic SWNTs. In general, the mixture ratio of metallic to semiconducting SWNTs is geometrically decided and independent of tube diameter as shown in Figure 6l. When we take the stability of cup structure on the top of SWNTs into consideration, however, it is known that the population of semiconducting SWNTs obviously increases[18] when the diameter is less than 1.0 nm, like in CoMoCAT SWNTs.[19] The PL quenching in sample (ii) through metallic SWNTs is, therefore, supposed to be much higher than that in sample (i), which results in low $\varepsilon_{m\text{-}EET}$. Although a significant increment of $\varepsilon_{m\text{-}EET}$ can be realized in sample (i), $\varepsilon_{m\text{-}EET}$ is lower than a reported value in a solution,[3] which is conjectured to originate from the imperfection of bundle formation in the air condition compared with that of a solution-phase reaction. The broad diameter distribution compared with the CoMoCAT SWNTs might also be attributed to low $\varepsilon_{m\text{-}EET}$. Actually, a slight depression of I_A/I_D is observed after several hours in sample (i) as seen in Figure 6k, which might indicate the quenching through metallic SWNTs.

The diameter distribution and efficient bundle formation are considered to be the important factors to realize high $\varepsilon_{m\text{-}EET}$. However, once ethanol was dropped on the substrate, the PL emission was immediately suppressed. When we attempted to measure the PL emission using as-grown SWNTs prepared with alcohol CVD,[20] any clear PL signals could not be detected. In our sample, on the contrary, the clear PL polarizability was still sustained even at 120 h after the growth. These facts claim the most important element to realize the PL brightening in the air

(17) See the Supporting Information for the diameter distribution estimation.

(18) Jorio, A.; Santos, A. P.; Ribeiro, H. B.; Fantini, C.; Souza, M.; Vieira, J. P. M.; Furtado, C. A.; Jiang, J.; Saito, R.; Balzano, L.; Resasco, D. E.; Pimenta, M. A. *Phys. Rev. B* **2005**, *72*, 075207.
(19) Bachilo, S. M.; Balzano, L.; Herrera, J. E.; Pompeo, F.; Resasco, D. E.; Weisman, R. B. *J. Am. Chem. Soc.* **2003**, *125*, 11186.
(20) Maruyama, S.; Kojima, R.; Miyauchi, Y.; Chiashi, S.; Kohno, M. *Chem. Phys. Lett.* **2002**, *360*, 229.

condition is the unique as-grown state (i.e., freestanding form), which can effectively avoid the PL quenching through the substrate. The diameter dependence on the PL brightening also includes the possibility of chirality dependency of $\varepsilon_{m\text{-}EET}$ on the combination of donor and acceptor tubes. The more concrete carrier dynamics of the PL brightening through EET and the quantitative comparison of the quantum yield between isolated and thin bundled SWNTs are still undiscovered. Further study of these issues is inevitable to realize the nanotube-based PL devices, and these studies are part of our future work.

Conclusions

PL brightening through the direct transition from isolated to bundled SWNTs has been observed using vertically and individually freestanding as-grown SWNTs as a starting material. The origin of broad-peak brightening is precisely investigated on the basis of the detailed spectral analysis and equation-based estimation for the time trace of PL spectra. The continuous change of integrated PL intensities between isolated and unknown broad peaks indicates that the EET through the tube bundle is the primal mechanism realizing the PL brightening. The obvious $\varepsilon_{m\text{-}EET}$ dependence on the morphology and diameter is also revealed. The critical answer for the PL emission from bundled SWNTs is the low metallic SWNT concentration and freestanding shape. The brightly luminescent dry materials consisting of freestanding thin-bundled SWNTs will open the door to realization of nanotube-based PL devices.

Acknowledgment. We thank Prof. K. Tohji and K. Motoniya for their technical support of the TEM measurement. This research was partly carried out at the Laboratory for Nanoelectronics and Spintronics, Research Institute of Electrical Communication, Tohoku University. T.K. was supported by Research Fellowships of the Japan Society for the Promotion of Science for Young Scientists.

Supporting Information Available: Experimental details for the polarized PL measurement. The estimation of the diameter distribution for sample (ii) in Figure 6. This material is available free of charge via the Internet at http://pubs.acs.org.

JA802427V